

Full paper

Large out-of-plane piezoelectricity of oxygen functionalized MXenes for ultrathin piezoelectric cantilevers and diaphragms



Jie Tan^{a,1}, Yunhua Wang^{b,e,*,1}, Zongtan Wang^c, Xiujie He^a, Yulan Liu^c, Biao Wang^{a,d,**}, Mikhail I. Katsnelson^e, Shengjun Yuan^{b,f,***}

^a Sino-French Institute of Nuclear Engineering and Technology, Sun Yat-sen University, Zhuhai, 519082, China

^b Beijing Computational Science Research Center, Beijing, 100193, China

^c School of Aeronautics and Astronautics, Sun Yat-sen University, Guangzhou, 510006, China

^d State Key Laboratory of Optoelectronic Materials and Technologies and School of Physics, Sun Yat-sen University, Guangzhou, 510275, China

^e Institute for Molecules and Materials, Radboud University, Heijendaalseweg 135, NL-6525, AJ, Nijmegen, The Netherlands

^f Key Laboratory of Artificial Micro- and Nano-structures of Ministry of Education and School of Physics and Technology, Wuhan University, Wuhan, 430072, China

ARTICLE INFO

Keywords:

MXenes

Piezoelectricity

Out-of-plane piezoelectricity

Piezoelectric charge density

Piezoelectric diaphragm

ABSTRACT

MXenes have currently drawn considerable attention in functional materials and energy storages, because of their versatile and excellent properties. However, few works have been made on MXenes' piezoelectricity. Applying the density-functional theory, we show that M_2CO_2 ($M = Sc, Y, La$) MXenes possess large Poisson's ratio and in-plane piezoelectricity comparable to that of $2H-MoS_2$. Furthermore, M_2CO_2 MXenes have strong out-of-plane piezoelectricity, which is highly desirable for ultrathin piezoelectric devices (cantilever and diaphragm) with the d_{31} operating mode. For a MXene diaphragm the piezoelectricity-generated charges mainly concentrate in six areas, which are determined by the lattice symmetry. In particular, the in-plane piezoelectric charges are localized near the circular clamped boundary, whereas the out-of-plane piezoelectric charges are inside the pressure-induced bubble. Our observations propose a realistic way to collect the piezoelectricity-induced charges, making these systems very promising for energy harvesting and piezoelectric sensing.

1. Introduction

MXenes, a new class of two-dimensional (2D) crystals, are experimentally extracted from the known MAX phase, i.e., a family of ternary carbides and nitrides, by etching the "A" layer in the MAX structure, where "M" is a transition metal, "A" is a group IIIA or IVA (i.e., groups 13 or 14) element, and "X" is C or N. The MXenes' chemical formula is usually written as $M_{n+1}X_nT_x$ ($n = 1-3$), where T_x is the surface terminations O, OH and/or F, naturally introduced into the pristine $M_{n+1}X_n$ during the acid etching process [1]. Since the synthesis of 2D titanium carbide in 2011 [2], MXenes have drawn considerable attention in functional materials and energy storages due to their versatile and excellent chemical and physical properties [1,3-7]. For chemical functional properties and applications, the high ion intercalation capacity and low intercalation voltages suggest MXenes (e.g., Ti_3C_2 [8,9], $Ti_3C_2T_x$ [9,10], V_2CT_x [11], Nb_2CT_x [11], and O-terminated M_2C with

$M = Sc, Ti, V, \text{ or } Cr$ [12]) as materials for ion intercalation batteries and supercapacitors; the large heavy metal sorption capacity makes MXenes (e.g., $Ti_3C_2(OH/ONa)_xF_{2-x}$ [13] and MXene-iron oxide [14]) useful for water purifications; and the molecular sieving effect makes MXenes (e.g., $Ti_3C_2T_x$) effective for gas separation [15]. For physical functional properties and applications, the metallic $Ti_3C_2T_x$ with high conductivity and large flexibility are used as a thin layer of electromagnetic interference shielding [16]; the functionalized M_2C with $M = Sc, Ti, Zr, \text{ and } Hf$, especially oxygenated M_2C , exhibit a semi-conducting behavior [17-19], which is favorable to field-effect transistors especially for biosensors owing to the hydrophilic surface property [20] and visible-light driven photocatalysts due to the large visible-light absorption as well as the efficient separations of photo-activated electron-hole pairs [21,22]; Mo_2C MXene and some double transition metal oxygen-functionalized carbides (or nitrides) MXenes display corresponding emergent quantum states, i.e., the 2D

* Corresponding author. Beijing Computational Science Research Center, Beijing, 100193, China.

** Corresponding author. Sino-French Institute of Nuclear Engineering and Technology, Sun Yat-sen University, Zhuhai, 519082, China.

*** Corresponding author. Beijing Computational Science Research Center, Beijing, 100193, China.

E-mail addresses: wangyunhua@csrc.ac.cn (Y. Wang), wangbiao@mail.sysu.edu.cn (B. Wang), s.yuan@whu.edu.cn (S. Yuan).

¹ J.T. and Y.W. contributed equally to this work.

<https://doi.org/10.1016/j.nanoen.2019.104058>

Received 18 June 2019; Received in revised form 12 August 2019; Accepted 27 August 2019

Available online 29 August 2019

2211-2855/© 2019 Elsevier Ltd. All rights reserved.

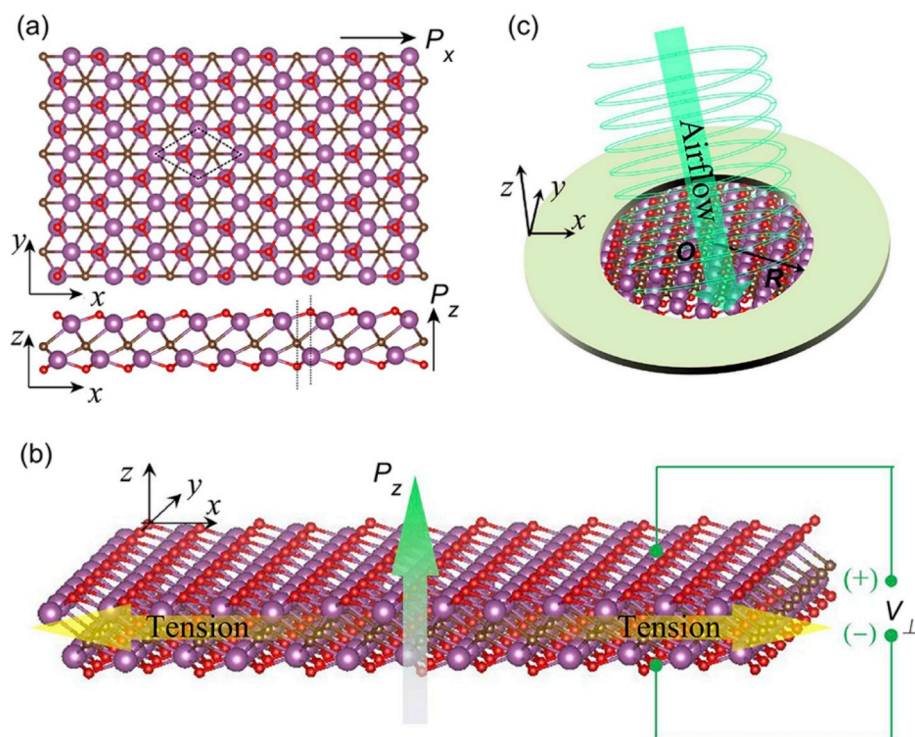


Fig. 1. (a) Crystal structures of Sc₂CO₂ MXene from the top view in x-y plane and the side view in x-z plane, where the purple, brown and red spheres represent the scandium, carbon and oxygen atoms, respectively. (b) A Sc₂CO₂ MXene cantilever. If the left end of the cantilever is clamped, it will suffer an opposite force due to the right uniaxial tension, and then a vertical piezoelectric voltage V_{\perp} is generated by the out-of-plane piezoelectric polarization P_z . (c) A Sc₂CO₂ MXene diaphragm with a radial symmetry and the clamped edge radius R , where a steady air-flow is applied to enable a uniform constant pressure in the vertical direction. (For interpretation of the references to color in this figure legend, the reader is referred to the Web version of this article.)

superconductivity [23] and topological insulators [24–27], and hence offer a research platform for new physics; some MXenes also exhibit ferromagnetic and antiferromagnetic features [28–31], with an application on spintronics; and the oxygen-functionalized scandium carbide monolayers have a switchable spontaneous polarization [32], which permits Sc₂CO₂ MXene to be ferroelectric or antiferroelectric states with applications on information storages.

In this context, a natural question arises whether MXenes also present some unique features in piezoelectricity, an another common but important physical functional property. The answer is affirmative for the 2D ordered double transition metals carbides with the largest in-plane piezoelectricity [33]. However, the piezoelectric feature for the semiconducting MXenes has not been studied yet. Generally, piezoelectricity is a linear cross-coupling between mechanical and electrical responses in non-centrosymmetric dielectric crystals. Owing to its high response sensitivity, robust and efficient transformation capability between electrical and mechanical signals (or energy), and simple technical feasibility, piezoelectricity is intensively applied in sensors, transducers and energy harvesting devices [34,35]. Recently, the birth of piezoelectricity in 2D materials has injected new vitality into the electromechanical coupling theories at nanoscale [36,37] and also paved a way towards embedding these new 2D piezoelectric materials in piezotronics, nano-electromechanical system and energy conversion system [38–41]. Hundreds of 2D materials are found to be piezoelectric, including, for instance, transition-metal dichalcogenides (TMDCs) [37,42–51] and oxides (TMDOs) [42,44], groups III [52,53] and IV [54–56] monochalcogenides, groups III-V semiconductors [42,57,58], modified graphene [59] and zinc oxide sheets [60]. Most of these known 2D piezoelectric materials only have an in-plane piezoelectricity. Only a fraction of them exhibit an out-of-plane piezoelectricity (e.g., the piezoelectric strain coefficient d_{31}). Usually, strong out-of-plane piezoelectric effect and its inverse effect are highly desirable for piezoelectric cantilever and diaphragm devices with the d_{31} piezoelectric mode, such as loudspeaker (and microphone) [61], sensor [62] and vibration energy harvesting [63,64]. This is because the cantilever and diaphragm structures are easy to vibrate back and forth, and the vertical piezoelectric polarization produced by the piezoelectricity is compatible with the bottom/top gate technologies.

Massive efforts have been made for searching 2D piezoelectric materials with large d_{31} , such as decorated graphene [59], Janus models of TMDCs [43], group-III chalcogenides [53], functionalized h-BN [65] and α -In₂Se₃ [66]. However, the out-of-plane piezoelectricity in these known 2D materials is weak.

Herein, we report the piezoelectric property of oxygen functionalized MXenes (labelled as M₂CO₂ with M = Sc, Y, and La), as depicted in Fig. 1a, where the noncentrosymmetric adsorption of oxygen atoms at the top and bottom surfaces breaks the original inversion symmetry of M₂C, and the hybridization between d orbitals of M atoms and p orbitals of O atoms induces a band gap. Both the broken inversion symmetry and semiconducting nature enable a considerable intrinsic piezoelectricity for M₂CO₂ MXenes. The density-functional perturbation theory calculations show that, M₂CO₂ MXenes have a remarkable flexibility, an in-plane piezoelectricity comparable to that of 2H-MoS₂ and the largest out-of-plane piezoelectricity among the known 2D materials. Especially, the piezoelectric strain coefficients d_{31} of Sc₂CO₂ MXene is up to 0.78 pm/V. This will result in a vertical piezoelectric voltage 0.1 V only inside an ultrathin thickness (0.38 nm) of Sc₂CO₂ monolayer under a 2.5% strain. We further make piezoelectric response simulations for a circular M₂CO₂ MXene diaphragm. The simulated results indicate that the nonuniform positive and negative charges produced by the in-plane piezoelectricity mainly concentrate in six regions near the clamped circular boundary but the out-of-plane piezoelectric charges are located inside the bubble. Therefore, our results give an experimental proposal for how to collect the piezoelectric charges induced by both the in-plane and out-of-plane piezoelectricity and pave a way for further designing MXene-based piezoelectric energy harvesting in near future.

2. Results and discussion

2.1. Crystal structure and device models of M₂CO₂ MXenes

Fig. 1a shows both the top and side views of the crystal structure of Sc₂CO₂ monolayer, as a representative of the 2D M₂CO₂ compounds, owing to their structural similarities. The overall honeycomb lattice consists of transition metal atoms, but the honeycomb lattice is actually

composed of the up and down triangular sub-lattice layers, as shown from the side view in the x - z plane. All these carbon atoms are inside the two layers of transition metal atoms. In addition, two oxygen atom layers are stably adsorbed at two non-equivalent sites: the low oxygen layer is just below the carbon atoms, and the up oxygen layer is directly above the next-nearest transition metal atoms. Such a 2D hexagonal structure clearly lacks an inversion center for both in-plane and out-of-plane directions. Therefore, these insulating M_2CO_2 monolayers have both the in-plane and out-of-plane piezoelectricity. If a tension along x axis is applied, the piezoelectric polarizations can appear along both x and z directions for the M_2CO_2 MXenes, where the armchair direction of transition metal atoms has been set as the x direction. Consequently, the corresponding piezoelectric stress tensor \mathbf{e} reads

$$\mathbf{e} = \begin{pmatrix} e_{11} & -e_{11} & 0 \\ 0 & 0 & -e_{11} \\ e_{31} & e_{31} & 0 \end{pmatrix}, \quad (1)$$

where e_{11} and e_{31} represent the in-plane and out-plane piezoelectric stress components in Voigt notation, respectively. The piezoelectric stress coefficients e_{11} and e_{31} are independent, and hence both of them need to be calculated. The stiffness tensor \mathbf{C} for the system reads

$$\mathbf{C} = \begin{pmatrix} C_{11} & C_{12} & 0 \\ C_{12} & C_{11} & 0 \\ 0 & 0 & C_{66} \end{pmatrix}, \quad (2)$$

where $C_{66} = (C_{11} - C_{12})/2$. Using $e_{lm} = d_{lk}C_{km}$, we can write the corresponding piezoelectric strain tensor components d_{11} and d_{31} as

$$d_{11} = e_{11}/(C_{11} - C_{12}), \quad d_{31} = e_{31}/(C_{11} + C_{12}). \quad (3)$$

The forms of these piezoelectric and stiffness constants in Eqs. (1)–(3) for M_2CO_2 MXenes are the same as those for TMDCs [45], because of the same D_{3h} ($6m2$) point group. It should be figured out that, in literatures there are usually two expressions for e_{26} and d_{26} with factors of 2 or 1/2, because the shear strain and stress with the corresponding factors are used in the definitions of piezoelectric coefficients, e.g., $e_{26} = -e_{11}/2$, $d_{26} = -d_{11}$ [42], and $e_{26} = -e_{11}$, $d_{26}/2 = -d_{11}$ [45]. However, the relation in Eq. (3) remains and hence there is no influence on calculation results of d_{11} and d_{31} . Fig. 1b shows a Sc_2CO_2 MXene cantilever. If a uniaxial tension is applied along the positive x axis, an opposite force will be produced at the left side for the cantilever with a clamped left terminal (which is not depicted for clarity). Consequently, the out-of-plane piezoelectricity will induce a vertical piezoelectric voltage V_{\perp} under the d_{31} mode. We also consider a Sc_2CO_2 MXene diaphragm with a radial symmetry, as shown in Fig. 1c. The diaphragm's edge is clamped with the radius R , and a vertical airflow is used to induce a uniform vertical pressure on this membrane. Here we consider a steady flow to guarantee a constant vertical pressure on the membrane. Due to the vertical pressure, the membrane is deformed with an out-of-plane displacement, and the polarizations and charges are generated by both in-plane and out-of-plane piezoelectricity. The generated piezoelectric voltage, polarizations and charge density for these devices will be studied later.

2.2. Band structures

In general, a piezoelectric material should have a band gap for prohibiting current leakage. Therefore, it is necessary to examine the electronic structures of M_2CO_2 monolayers before the piezoelectric calculations. It is known that PBE functional is effective to estimate the electronic properties but usually underestimates the band gap of a material. The alternative HSE hybrid functional can supply more accurate calculations on electronic structures. Consequently, here we adopt the HSE functional with 25% exact exchange to calculate the band structures of M_2CO_2 monolayers, as plotted in Fig. 2. The up conduction bands and down valence bands near the Fermi energy for

M_2CO_2 MXenes are mainly contributed by both the d orbitals of metal atoms and the p orbitals of C and O atoms. It is different from that for transition metal dichalcogenide monolayers such as 2H-MoS₂, where the contributions from p orbitals of S atoms are weak near the Fermi energy [67–69]. The HSE functional results show that the band gaps for Sc_2CO_2 , Y_2CO_2 and La_2CO_2 are 2.86 eV, 2.34 eV and 1.29 eV, respectively. Therefore, M_2CO_2 MXenes are good semiconductors for piezoelectricity with relatively large band gaps.

2.3. Elastic properties

The relation between piezoelectric strain and stress tensors is connected by the elastic stiffness tensor, i.e., $e_{lm} = d_{lk}C_{km}$. Therefore, after the calculations of band structures, we need to further calculate the elastic stiffness coefficients to determine their piezoelectric properties. It is a fact that any one single crystal is comprised of ionic cores and electrons. Naturally, the mechanical and piezoelectric properties contain both electronic and ionic contributions. An effective method for separating the electronic and relaxation contributions to piezoelectricity is the clamped-ion and relaxed-ion models. The clamped-ion model neglects the ionic internal displacements and hence only contains the electronic contribution. The relaxed-ion model is corresponding to the experimental value. Therefore, the ionic contribution is the difference between the relaxed-ion and clamped-ion results. The elastic stiffness coefficients (C_{12} and C_{11} , with $C_{11} = C_{22}$ for a hexagonal lattice), Poisson's ratios (i.e., $\nu = C_{12}/C_{11}$) and Young's modulus (i.e., $Y = (C_{11}^2 - C_{12}^2)/C_{11}$) of M_2CO_2 monolayers for both the relaxed-ion and clamped-ion cases are obtained after optimizing the geometries, and their values are listed in Table 1. The ionic internal relaxation releases part of stress in the relaxed-ion case, and hence the real elastic stiffness coefficients are less than those for the clamped-ion case. As seen in Table 1, these elastic stiffness coefficients satisfy the Born criteria of 2D hexagonal structures, i.e., $C_{11} > 0$, and $C_{11} - C_{12} > 0$ [70], thereby ensuring their mechanical stabilities. In addition, C_{11} , C_{12} and Y decrease with an increase of the atomic number for the transition metal atom. The single layer Sc_2CO_2 among these M_2CO_2 monolayers has the maximum Young's modulus (120 N/m), which is smaller than that of BN (275.9 N/m) and graphene (341 N/m) [71,72], but can be comparable to that of monolayer TMDCs (103–139 N/m) [71]. The calculated results also show that the M_2CO_2 monolayers possess large Poisson's ratios more than that of rubber (~ 0.5) and 2D ZrO₂ [44]. The small Young's modulus and the large Poisson's ratios indicate that M_2CO_2 MXenes are easy to be deformed. Therefore, M_2CO_2 MXenes are very favorable for novel flexible piezotronics and nanoelectronics.

2.4. In-plane piezoelectricity

Fig. 3 shows the calculated results of piezoelectric stress coefficient e_{11} and strain coefficient d_{11} for M_2CO_2 monolayers ($M = Sc, Y, La$) for both clamped-ion and relaxed-ion cases. The corresponding piezoelectric values for h -BN and MoS₂ monolayers in available data [45] are also listed for comparison. As we can see, the relaxed-ion piezoelectric results are positive and the clamped-ion results are negative. This means that the electronic and ionic polarizations for these materials have obviously opposite signs. In addition, in view of the fact that the real piezoelectric value (a relaxed-ion result) is the sum of ionic contribution and electronic contribution (a clamped-ion result), from Fig. 3 we can conclude that the ionic contribution to the in-plane piezoelectricity should be much larger than the electronic contribution for M_2CO_2 MXenes. This feature is quite different from that of MoS₂, where the electronic contributions dominate the in-plane piezoelectricity [45,51]. From Sc_2CO_2 to Y_2CO_2 and then to La_2CO_2 , the piezoelectricity increases with the increasing atomic number of the transition metal atoms. The real piezoelectric coefficients (i.e., relaxed-ion cases) of Sc_2CO_2 ($e_{11} = 2.69 \times 10^{-10}$ C/m, $d_{11} = 3.41$ pm/V) are close to those of MoS₂ ($e_{11} = 3.64 \times 10^{-10}$ C/m, $d_{11} = 3.73$ pm/V) [45], but larger than those for h -BN ($e_{11} = 1.38 \times 10^{-10}$ C/m, $d_{11} = 0.6$ pm/V) [45] and 2D

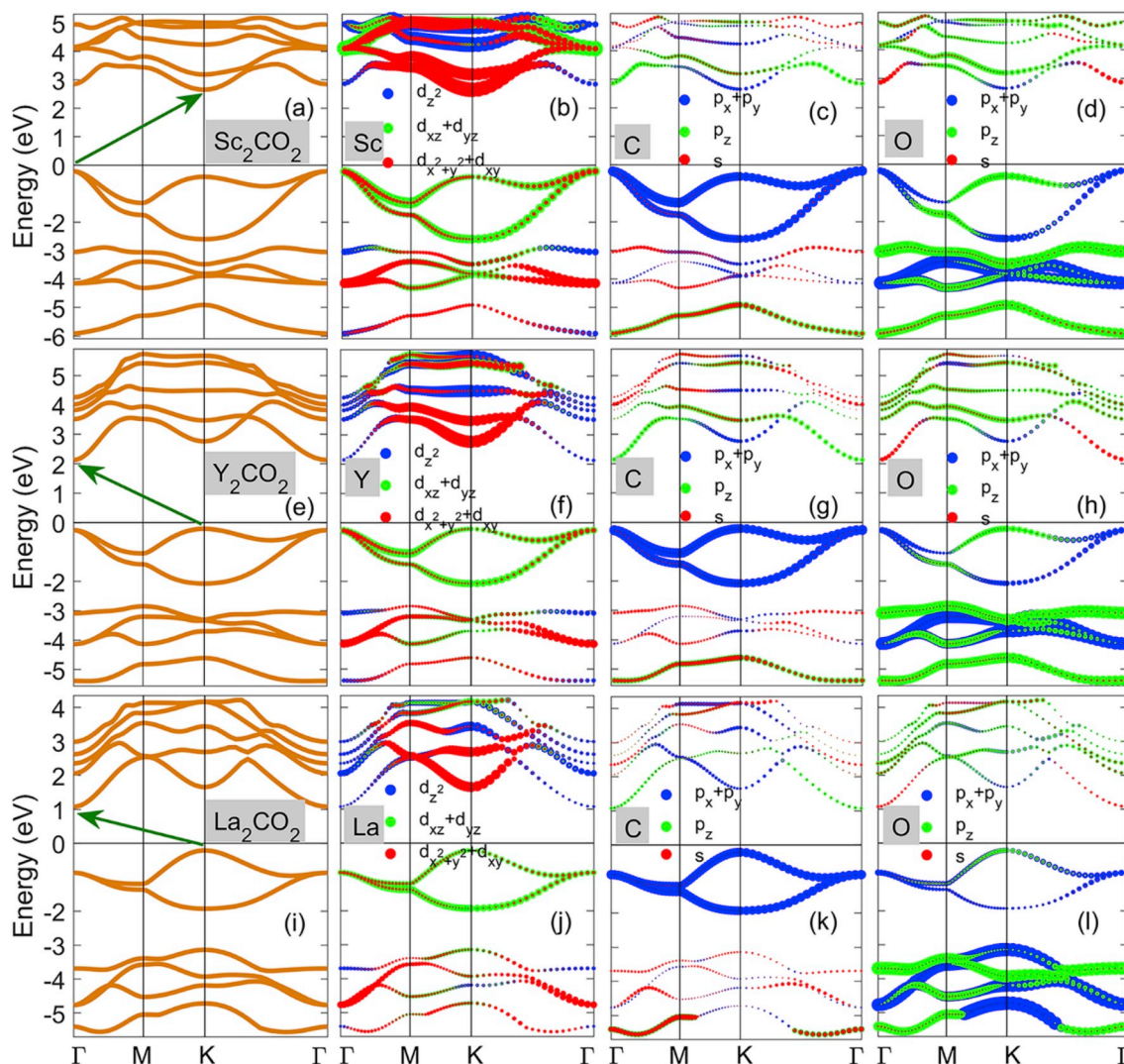


Fig. 2. Calculated Band structures of M_2CO_2 monolayers from the HSE hybrid functional. Band structures for (a) Sc_2CO_2 , (e) Y_2CO_2 , and (i) La_2CO_2 , respectively. Contributions from d orbitals for (b) Sc, (f) Y, and (j) La, respectively. Contributions from s and p orbitals of C in (c) Sc_2CO_2 , (g) Y_2CO_2 , and (k) La_2CO_2 , respectively. Contributions from s and p orbitals of O in (d) Sc_2CO_2 , (h) Y_2CO_2 , and (l) La_2CO_2 , respectively. Here, the Fermi energy is set to zero.

Table 1

Calculated clamped-ion and relaxed-ion elastic stiffnesses C_{11} and C_{12} , Young's modulus (Y) and Poisson's ratios (ν) for M_2CO_2 MXenes.

Materials	Clamped-ion				Relaxed-ion			
	C_{11}	C_{12}	Y	ν	C_{11}	C_{12}	Y	ν
	(N·m ⁻¹)				(N·m ⁻¹)			
Sc_2CO_2	211	94	169	0.445	165	86	120	0.521
Y_2CO_2	183	81	147	0.443	142	78	99	0.549
La_2CO_2	148	81	103	0.547	107	77	52	0.719

graphitic carbon nitride ($g-C_3N_4$ with $e_{11} = 1.0 \times 10^{-10}$ C/m) [73]. The piezoelectric coefficients of Y_2CO_2 ($e_{11} = 3.92 \times 10^{-10}$ C/m, $d_{11} = 6.16$ pm/V) and La_2CO_2 ($e_{11} = 6.81 \times 10^{-10}$ C/m, $d_{11} = 22.32$ pm/V) monolayers are obviously larger than those for transition metal dichalcogenide monolayers ($e_{11} = 2.47\text{--}3.92 \times 10^{-10}$ C/m, $d_{11} = 2.19\text{--}9.13$ pm/V) [45], group III monochalcogenides ($e_{11} = 0.57\text{--}1.47 \times 10^{-10}$ C/m, $d_{11} = 1.46\text{--}2.30$ pm/V) [52], Janus group III chalcogenide monolayers ($e_{11} = 0.67\text{--}3.60 \times 10^{-10}$ C/m, $d_{11} = 1.18\text{--}8.47$ pm/V) [53], group VI buckled monolayers ($e_{11} = 0.15\text{--}1.57 \times 10^{-10}$ C/m, $d_{11} = 0.33\text{--}5.42$ pm/V

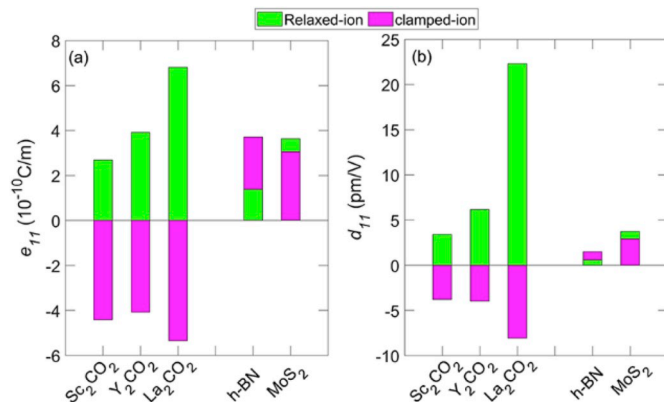


Fig. 3. Calculated piezoelectric stress coefficient e_{11} in (a) and strain coefficient d_{11} in (b) for M_2CO_2 ($M = Sc, Y, La$) MXenes under both clamped-ion and relaxed-ion cases. Here the corresponding coefficients of $h\text{-BN}$ and MoS_2 [45] are also listed for comparison.

V) [74], group III-V compounds ($e_{11} = 0\text{--}2.40 \times 10^{-10}$ C/m, $d_{11} = 0\text{--}5.5$ pm/V) [42] and most of group II-VI semiconductor monolayers ($e_{11} = 0.09\text{--}3.18 \times 10^{-10}$ C/m, $d_{11} = 1.04\text{--}23.8$ pm/V) [75].

Table 2
Calculated piezoelectric coefficients e_{31} and d_{31} for M_2CO_2 ($M = Sc, Y, La$) MXenes under both the clamped-ion and relaxed-ion cases.

Materials	Clamped-ion		Relaxed-ion	
	e_{31} (pC·m ⁻¹)	d_{31} (pm·V ⁻¹)	e_{31} (pC·m ⁻¹)	d_{31} (pm·V ⁻¹)
Sc ₂ CO ₂	116	0.38	196	0.78
Y ₂ CO ₂	4.22	0.02	88	0.40
La ₂ CO ₂	-0.47	-0.002	120	0.65

2.5. Out-of-plane piezoelectricity

The asymmetric oxygen adsorption along the z direction also results in an out-of-plane piezoelectricity for M_2CO_2 monolayers. This means that an in-plane stress or strain would induce a polarization change vertical to the plane. A large out-of-plane piezoelectric response is highly desired for 2D materials, since it not only adds an additional spatial piezoelectric degree of freedom but also is compatible with the nowadays bottom/top gate technologies. Therefore, we further calculate the out-of-plane piezoelectric coefficients e_{31} and d_{31} for M_2CO_2 MXenes under both clamped-ion and relaxed-ion cases and list their values in Table 2. For Sc₂CO₂ monolayer, the electronic and ionic contributions to the out-of-plane piezoelectricity have the same signs and comparable magnitudes. However, for Y₂CO₂ and La₂CO₂, the out-of-plane piezoelectricity is mainly determined by the ionic contributions because the electronic contribution from the clamped-ion calculations vanishes dramatically as shown in Table 2. The relaxed-ion piezoelectric strain coefficients (d_{31}) have large values: 0.78 pm/V, 0.40 pm/V, and 0.65 pm/V for Sc₂CO₂, Y₂CO₂, and La₂CO₂, respectively. The out-of-plane piezoelectricity d_{31} of M_2CO_2 MXenes is obviously higher compared with other 2D known materials, including the Janus transition metal dichalcogenide monolayers (0.03 pm/V) [43], functionalized *h*-BN (0.13 pm/V) [65], kalium decorated graphene (0.3 pm/V) [59], Janus group-III materials (0.46 pm/V) [53], and α -In₂Se₃ (0.415 pm/V) [66]. Especially, Sc₂CO₂ monolayer has the largest out-of-plane d_{31} (0.78 pm/V) among all atomic-thick 2D materials, to the best of our knowledge. The large out-of-plane piezoelectric effect together with high flexibility would endow these M_2CO_2 MXenes potential applications on ultrathin piezoelectric cantilever and diaphragm devices. It should be noted that there is an obvious difference between piezoelectric coefficients d_{33} and d_{31} even though both of them are related to the out-of-plane piezoelectric polarization. The coefficient d_{33} represents the piezoelectric response between the out-of-plane polarization and the out-of-plane deformation, while d_{31} is referred to as the coupling between the out-of-plane polarization and the in-plane deformation. In previous piezoresponse force microscopy (PFM) experiments [47,73], the coefficient d_{33} for 2D g-C₃N₄ and MoS₂ is measured by checking the out-of-plane deformation resulting from a vertical electric field. However, the in-plane deformation should be examined to measure d_{31} for M_2CO_2 MXenes.

2.6. Piezoelectric voltage in a M_2CO_2 MXene cantilever

Assuming that the charges generated by the in-plane piezoelectricity satisfy a model of two parallel line charges, one can write the voltage across the plane as $V_{\parallel} = (P_x/\pi\xi)\ln(L/a)$ [76], where the armchair edge is defined as the x axis, P_x is the x-directional piezoelectric polarization, ξ is the dielectric constant, L is the x-directional distance between the two line charges, and the radius a of the line is supposed to be the lattice constant. However, the line charge model is not suitable for the out-of-plane piezoelectricity. Fig. 1b shows the d_{31} piezoelectric model of M_2CO_2 MXenes, where the left clamped end of the cantilever suffers an opposite force due to the uniaxial tension. An out-of-plane voltage is induced by the vertical (out-of-plane) piezoelectric polarization P_z . The vertical piezoelectric voltage V_{\perp} is approximately described by a

capacitor model with top and bottom parallel plates. Consequently, the vertical voltage reads

$$V_{\perp} = \frac{P_z}{\xi} = \frac{(1-\nu)e_{31}\varepsilon_{xx}}{\xi} = \frac{(1-\nu)(C_{11} + C_{12})d_{31}\varepsilon_{xx}}{\xi} \quad (4)$$

where $P_z = (\varepsilon_{xx} + \varepsilon_{yy})e_{31}$ is the z-directional polarization with $\varepsilon_{yy} = -\nu\varepsilon_{xx}$, ν is the Poisson's ratio, and ξ should be the dielectric constant of M_2CO_2 monolayer because the vertical electric field passes through the material itself. Notice that Eq. (4) is only valid for in-plane uniform deformation. Eq. (4) shows that V_{\perp} is determined by the intrinsic elastic and dielectric properties in a cantilever structure for a fixed strain ε_{xx} . Therefore, the quantity $g_{31} = (1-\nu)e_{31}/\xi$ is effective to compare the voltage V_{\perp} in a cantilever for different 2D materials with D_{3h} (6m2) point group. We take a Sc₂CO₂ monolayer as an example, where $\xi = 2.51\xi_0$ [77] with the vacuum dielectric constant ξ_0 , $\nu = 0.521$ in Table 1, and $e_{31} = 196$ pC/m in Table 2. According to Eq. (4) the voltage can be estimated by $V_{\perp} \sim 4\varepsilon_{xx}$ with the unit of V in the Sc₂CO₂ MXene cantilever. Usually, many 2D materials can sustain a large elastic strain higher than 15% owing to their membrane's features. We also check that the largest strain for MXenes, for instance, the elastic strain limits are 14% and 17% along the armchair (x) and zigzag (y) directions, respectively, for Sc₂CO₂ monolayers (Fig. S1 in Supplementary material I). Therefore, even for a relatively moderate strain, a considerable voltage can be generated by the out-of-plane piezoelectricity in M_2CO_2 MXenes, which are suitable for the d_{31} mode piezoelectric devices with the bottom/top gates and an ultrathin thickness less than 1 nm. In addition, one can further design multi MXene layers separated by flexible insulating medium to enlarge the total voltage.

2.7. Piezoelectric charge density in a M_2CO_2 MXene diaphragm

Generally, it is difficult to make an analytical expression for both the in-plane and out-of-plane piezoelectric voltages for a 2D piezoelectric diaphragm, because both the polarization and charge density are nonuniform during the deformation process. However, the analysis of piezoelectric polarizations and charge density distributions can suggest where the positive and negative electrodes should be in order to collect the charges for energy storage and piezoelectric sensing. Fig. 4 show the piezoelectric charge density distribution on the 2D M_2CO_2 piezoelectric diaphragm under the airflow, as depicted in Fig. 1c. Obviously, these charge densities are nonuniform. In Fig. 4a, the positive and negative charges generated by the in-plane piezoelectricity mainly concentrate in six regions near the clamped boundary, i.e., $r \sim R$. In Fig. 4b, the charges generated by the out-of-plane piezoelectricity are also located in six regions but inside the circle, i.e., $r < R$. In addition, from the charge density's magnitude denoted by the color bars, we can see that the charge density generated by the out-of-plane piezoelectricity is obviously larger than that generated by the in-plane piezoelectricity. These positive charges are inside the golden areas and these negative charges lie in the blue areas. Therefore, for the M_2CO_2 MXene bubble in Fig. 4c, the golden and blue areas are suitable to be touched the positive and negative electrodes, respectively, to collect these piezoelectricity-generated charges for piezoelectric sensing and energy harvesting. The piezoelectric polarization fields determining the charge density are also calculated and plotted in Fig. S2. Eqs. (8)-(10) indicate that the charge density is dependent on the factor $\cos(3\theta)$, which is determined by the lattice symmetry of M_2CO_2 MXene. If θ is defined as the angle between the radial direction and zigzag edge, the charge density is a function of $\sin(3\theta)$, because there is an angle difference of 30° between zigzag and armchair edges. We also estimate the size of piezoelectricity-generated charge density. We consider Sc₂CO₂ MXene as an example. For Sc₂CO₂ MXene, the previous calculations show that, $\nu = 0.521$, $e_{11} = 2.69 \times 10^{-10} \text{C}\cdot\text{m}^{-1}$, and $e_{31} = 1.16 \times 10^{-10} \text{C}\cdot\text{m}^{-1}$. According to $\rho_0 = (1+\nu)h_0^2 e_{11}/R^3$ given in

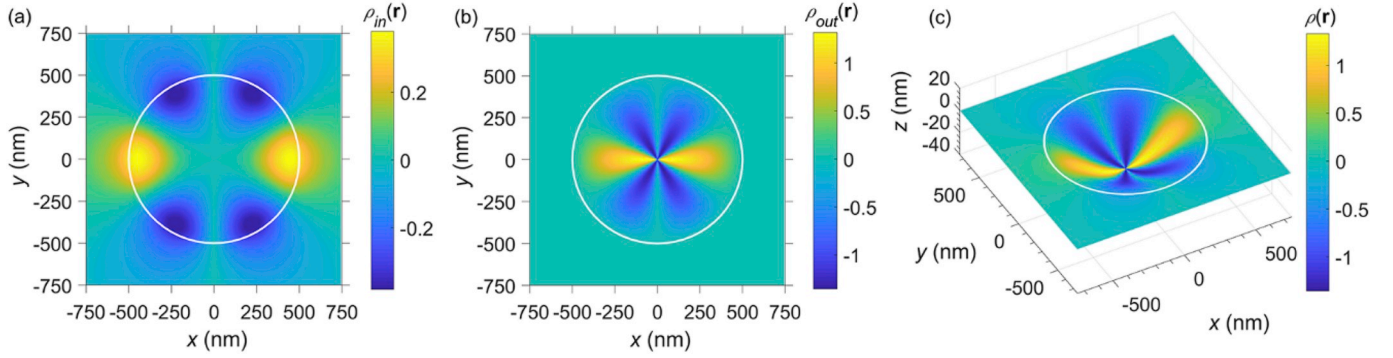


Fig. 4. (a) Calculated charge density $\rho_{in}(\mathbf{r})$ induced by the in-plane piezoelectricity in Eq. (8) from the top view, (b) Calculated charge density $\rho_{out}(\mathbf{r})$ induced by the out-of-plane piezoelectricity in Eq. (9) from the top view, and (c) Calculated total charge density $\rho(\mathbf{r})$ in Eq. (10) for the MXene bubble generated by the airflow shown in Fig. 1c. Here, $a = -1$, $b = -0.5$, $R = 500\text{nm}$, $h_0 = 50\text{nm}$, and all the charge densities are rescaled with the same unit ρ_0 . The white circle is the clamped edge.

method section, the charge density is estimated to be $(0.51 \times 10^{10}\text{cm}^{-2})e$ with the elementary charge e , for a diaphragm with typically experimental parameters $R = 500\text{nm}$ and $h_0 = 50\text{nm}$.

3. Conclusions

In conclusion, based on the density-functional theory, we investigate the electronic structures, elastic properties and piezoelectric properties for M_2CO_2 ($\text{M} = \text{Sc}, \text{Y}, \text{La}$) MXenes. M_2CO_2 monolayers have a larger Poisson's ratio than rubber. The clamped- and relaxed-ion model calculations show that M_2CO_2 monolayers have large in-plane and out-of-plane piezoelectricity, which mainly results from the ionic contributions. Especially, Sc_2CO_2 MXene has the largest out-of-plane piezoelectricity with its $d_{31} = 0.78 \text{ pm/V}$ among the known 2D materials. Therefore, M_2CO_2 MXenes are very suitable for ultrathin piezoelectric devices under the d_{31} operating mode. We construct a vertical piezoelectric voltage formula for a M_2CO_2 MXene cantilever. We also perform the piezoelectric response simulations on the charge density in a circular piezoelectric MXene diaphragm. The simulation results indicate that, the charges generated by both the in-plane and out-of-plane piezoelectricity concentrate in six regions determined by the lattice symmetry of M_2CO_2 MXene. The in-plane piezoelectric charges mainly distribute near the clamped boundary, but the out-of-plane piezoelectric charges are located inside the bubble. Therefore, our results not only supply an experimental proposal for how to detect the piezoelectric responses, but also offer an insight into piezoelectric energy harvesting and sensing based on MXenes.

4. Calculation setup

4.1. Calculation details of DFT

The present calculations are performed within the framework of density functional theory in VASP [78,79]. Exchange and correlation effects were treated self-consistently with a generalized gradient approximation (GGA) using a Perdew-Burke-Ernzerhof (PBE) exchange-correlation functional [80]. Electron-ion interactions were described by the projector augmented plane-wave method [81,82]. Electron wavefunctions were expanded in a plane-wave basis set with an energy cutoff of 600 eV. For structure optimization, a conjugate gradient scheme without any symmetry restrictions was used for the total energy and Hellmann-Feynman forces to converge to within 10^{-7} eV and 0.005 eV/\AA , respectively. The Brillouin zone was sampled on grids of $24 \times 24 \times 1$ within the gamma center scheme. In order to prevent the periodic interaction along the z-direction, 20 \AA of vacuum space was set between the neighboring layers. A high precision and computationally more expensive Heyd-Scuseria-Ernzerhof (HSE) hybrid functional [83] was employed to calculate the electronic structure of the GGA-PBE

optimized phases. The coefficients of the elastic stiffness tensor and the piezoelectric tensor were obtained using density-functional perturbation theory [84,85], which has been shown to give a successful estimate of the piezoelectric properties for a wide range of materials [86]. Here, a highly dense k-point mesh, $36 \times 36 \times 1$, was used to accurately predict these tensor components.

4.2. Calculation details of piezoelectric charge density

We carry out the analysis of the charge density for a diaphragm structure of M_2CO_2 MXenes with a radial symmetry and a clamped edge radius R , as shown in Fig. 1c, where a steady airflow enables a uniform vertical pressure on the 2D membrane. The in-plane displacement reads $(\cos \theta, \sin \theta)u(r)$, where $u(r)$ is the radial displacement as a function of the radius r , and θ is the angle between the radial vector and the armchair edge along the x axis. The deflection (i.e., out-of-plane displacement) usually takes a parabolic function of the radius r ($0 \leq r \leq R$), i.e., $h(r) = h_0(1 - (r/R)^2)^2$ [87], where h_0 is height of the plate center. Experiments and finite element simulations show that for a 2D material under a vertical pressure a modified parabolic profile is a good approximation [88–90], for $h_0 \ll 2R$, namely, $10h_0 < 2R$. Therefore, we write the modified parabolic profile for M_2CO_2 MXenes as

$$h(r) = \Theta(R - r)h_0[(a - b) - a(r/R)^2 + b(r/R)^4], \quad (5)$$

where $\Theta(x)$ is the Heaviside step function, and the three parameters a , b and h_0 determine the deflection profile. The piezoelectric tensor of M_2CO_2 MXene connects the polarization \mathbf{P} with the strain $\boldsymbol{\epsilon}$ in a cylindrical coordinate system (Supplementary materials II and III), as follows:

$$\begin{cases} P_x = e_{11}(\epsilon_{rr} - \epsilon_{\theta\theta})\cos(2\theta), \\ P_y = e_{11}(\epsilon_{\theta\theta} - \epsilon_{rr})\sin(2\theta), \\ P_z = e_{31}(\epsilon_{rr} + \epsilon_{\theta\theta}), \end{cases} \quad (6)$$

where θ is the azimuth angle, and the strain components ϵ_{rr} and $\epsilon_{\theta\theta}$ are a function of the in-plane radial displacement $u(r)$ and the deflection $h(r)$ with the following expressions:

$$\epsilon_{rr} = \frac{du(r)}{dr} + \frac{1}{2} \left[\frac{dh(r)}{dr} \right]^2, \quad \epsilon_{\theta\theta} = \frac{u(r)}{r}. \quad (7)$$

Because the linear piezoelectric effect mainly induces the charge for a relatively small out-of-plane displacement, here we neglect the weak strain gradient effect on the polarization. Although there is no need to distinguish which charges are induced by the in-plane piezoelectricity and which charges are induced by the out-of-plane piezoelectricity in experiments, it is convenient to divide the charges into two parts for theoretical analysis. Using $\rho(\mathbf{r}) = -\nabla \cdot \mathbf{P}$, we can obtain the charge density $\rho_{in}(\mathbf{r})$ induced by the in-plane piezoelectricity, the charge density $\rho_{out}(\mathbf{r})$ induced by the out-of-plane piezoelectricity and the total

charge density $\rho(\mathbf{r})$, respectively, as follows (Supplementary material III):

$$\rho_{in}(\mathbf{r}) = \rho_0 \left[\left(\frac{8abr^3}{3R^3} - \frac{4b^2r^5}{R^5} \right) \Theta(R-r) + \frac{(6a^2 - 16ab + 12b^2)R^3}{3r^3} \Theta(r-R) \right] \cos(3\theta), \quad (8)$$

$$\rho_{out}(\mathbf{r}) = \rho_{z,0} [-a + 2b(r/R)^2] \Theta(R-r) \cos(3\theta), \quad (9)$$

$$\rho(\mathbf{r}) = \rho_{in}(\mathbf{r}) + \rho_{out}(\mathbf{r}), \quad (10)$$

where $\rho_0 = (1 + \nu)h_0^2e_{11}/R^3$, and $\rho_{z,0} = (1 - \nu)h_0e_{31}/R^2$. It is convenient to rescale $\rho_{out}(\mathbf{r})$ with the same unit ρ_0 as $\rho_{in}(\mathbf{r})$ by rewriting $\rho_{z,0} = (\rho_{z,0}/\rho_0)\rho_0$. It should also be mentioned that the simulation methods can be further extended to dynamical systems with a time-dependent pressure, if we know the time-dependent expressions of parameters a , b and h_0 .

Acknowledgements

This work was supported financially by the National Natural Science Foundation of China (Grant Nos. 11502308, 11832019, 11472313, 11502130, 11572355, and U1930402), the National Key R&D Program of China (Grant No. 2018FYA0305800), and the Natural Science Foundation of China Guangdong Province (Grant No. 2016A030310205).

Appendix A. Supplementary data

Supplementary data to this article can be found online at <https://doi.org/10.1016/j.nanoen.2019.104058>.

References

- [1] B. Anasori, M.R. Lukatskaya, Y. Gogotsi, 2D metal carbides and nitrides (MXenes) for energy storage, *Nat Rev Mater* 2 (2017) 16098.
- [2] M. Naguib, M. Kurtoglu, V. Presser, J. Lu, J. Niu, M. Heon, L. Hultman, Y. Gogotsi, M.W. Barsoum, Two-dimensional nanocrystals produced by exfoliation of Ti_3AlC_2 , *Adv. Mater.* 23 (2011) 4248–4253.
- [3] M. Naguib, V.N. Mochalin, M.W. Barsoum, Y. Gogotsi, 25th anniversary article: MXenes: a new family of two-dimensional materials, *Adv. Mater.* 26 (2014) 992–1005.
- [4] Y. Zhong, X. Xia, F. Shi, J. Zhan, J. Tu, H.J. Fan, Transition metal carbides and nitrides in energy storage and conversion, *Adv. Sci.* 3 (2016) 1500286.
- [5] H. Kim, Z. Wang, H.N. Alshareef, MXene: electronic and photonic applications of MXenes, *Nano Energy* 60 (2019) 179–197.
- [6] K. Hantanasirisakul, Y. Gogotsi, Electronic and optical properties of 2D transition metal carbides and nitrides (MXenes), *Adv. Mater.* 30 (2018) e1804779.
- [7] M. Khazaei, M. Arai, T. Sasaki, C.Y. Chung, N.S. Venkataraman, M. Estili, Y. Sakka, Y. Kawazoe, Novel electronic and magnetic properties of two-dimensional transition metal carbides and nitrides, *Adv. Funct. Mater.* 23 (2013) 2185–2192.
- [8] M.R. Lukatskaya, O. Mashtalir, C.E. Ren, Y. Dall'Agnese, P. Rozier, P.L. Taberna, M. Naguib, P. Simon, M.W. Barsoum, Y. Gogotsi, Cation intercalation and high volumetric capacitance of two-dimensional titanium carbide, *Science* 341 (2013) 1502–1505.
- [9] Q. Tang, Z. Zhou, P. Shen, Are MXenes promising anode materials for Li ion batteries? Computational studies on electronic properties and Li storage capability of Ti_3C_2 and $\text{Ti}_3\text{C}_2\text{X}_2$ ($X = \text{F}, \text{OH}$) monolayer, *J. Am. Chem. Soc.* 134 (2012) 16909–16916.
- [10] M.R. Lukatskaya, S. Kota, Z.F. Lin, M.Q. Zhao, N. Shpigel, M.D. Levi, J. Halim, P.L. Taberna, M. Barsoum, P. Simon, Y. Gogotsi, Ultra-high-rate pseudocapacitive energy storage in two-dimensional transition metal carbides, *Nat Energy* 2 (2017) 17105.
- [11] M. Naguib, J. Halim, J. Lu, K.M. Cook, L. Hultman, Y. Gogotsi, M.W. Barsoum, New two-dimensional niobium and vanadium carbides as promising materials for Li-ion batteries, *J. Am. Chem. Soc.* 135 (2013) 15966–15969.
- [12] C. Eames, M.S. Islam, Ion intercalation into two-dimensional transition-metal carbides: global screening for new high-capacity battery materials, *J. Am. Chem. Soc.* 136 (2014) 16270–16276.
- [13] Q. Peng, J. Guo, Q. Zhang, J. Xiang, B. Liu, A. Zhou, R. Liu, Y. Tian, Unique lead adsorption behavior of activated hydroxyl group in two-dimensional titanium carbide, *J. Am. Chem. Soc.* 136 (2014) 4113–4116.
- [14] Q. Zhang, J. Teng, G. Zou, Q. Peng, Q. Du, T. Jiao, J. Xiang, Efficient phosphate sequestration for water purification by unique sandwich-like MXene/magnetic iron oxide nanocomposites, *Nanoscale* 8 (2016) 7085–7093.
- [15] L. Ding, Y. Wei, L. Li, T. Zhang, H. Wang, J. Xue, L.X. Ding, S. Wang, J. Caro, Y. Gogotsi, MXene molecular sieving membranes for highly efficient gas separation, *Nat. Commun.* 9 (2018) 155.
- [16] F. Shahzad, M. Alhabeib, C.B. Hatter, B. Anasori, S. Man Hong, C.M. Koo, Y. Gogotsi, Electromagnetic interference shielding with 2D transition metal carbides (MXenes), *Science* 353 (2016) 1137–1140.
- [17] Y. Lee, S.B. Cho, Y.C. Chung, Tunable indirect to direct band gap transition of monolayer Sc_2CO_2 by the strain effect, *ACS Appl. Mater. Interfaces* 6 (2014) 14724–14728.
- [18] G.R. Berdiyrov, Effect of surface functionalization on the electronic transport properties of Ti_3C_2 MXene, *Europhys. Lett.* 111 (2015) 67002.
- [19] M. Khazaei, A. Ranjbar, M. Arai, T. Sasaki, S. Yunoki, Electronic properties and applications of MXenes: a theoretical review, *J. Mater. Chem. C* 5 (2017) 2488–2503.
- [20] B. Xu, M. Zhu, W. Zhang, X. Zhen, Z. Pei, Q. Xue, C. Zhi, P. Shi, Ultrathin MXene-micropattern-based field-effect transistor for probing neural activity, *Adv. Mater.* 28 (2016) 3333–3339.
- [21] H.J. Zhang, G. Yang, X.Q. Zuo, H.B. Tang, Q. Yang, G. Li, Computational studies on the structural, electronic and optical properties of graphene-like MXenes (M_2CT_2 , $\text{M} = \text{Ti}, \text{Zr}, \text{Hf}$; $\text{T} = \text{O}, \text{F}, \text{OH}$) and their potential applications as visible-light driven photocatalysts, *J. Mater. Chem.* 4 (2016) 12913–12920.
- [22] Y.L. Bai, K. Zhou, N. Srikanth, J.H.L. Pang, X.D. He, R.G. Wang, Dependence of elastic and optical properties on surface terminated groups in two-dimensional MXene monolayers: a first-principles study, *RSC Adv.* 6 (2016) 35731–35739.
- [23] C. Xu, L. Wang, Z. Liu, L. Chen, J. Guo, N. Kang, X.L. Ma, H.M. Cheng, W. Ren, Large-area high-quality 2D ultrathin Mo_2C superconducting crystals, *Nat. Mater.* 14 (2015) 1135–1141.
- [24] H.M. Weng, A. Ranjbar, Y.Y. Liang, Z.D. Song, M. Khazaei, S. Yunoki, M. Arai, Y. Kawazoe, Z. Fang, X. Dai, Large-gap two-dimensional topological insulator in oxygen functionalized MXene, *Phys. Rev. B* 92 (2015) 075436.
- [25] C. Si, K.H. Jin, J. Zhou, Z. Sun, F. Liu, Large-gap quantum spin Hall state in MXenes: d-band topological order in a triangular lattice, *Nano Lett.* 16 (2016) 6584–6591.
- [26] M. Khazaei, A. Ranjbar, M. Arai, S. Yunoki, Topological insulators in the ordered double transition metals $\text{M}_2\text{M}'\text{C}_2$ MXenes ($\text{M}' = \text{Mo}, \text{W}$; $\text{M} = \text{Ti}, \text{Zr}, \text{Hf}$), *Phys. Rev. B* 94 (2016) 125152.
- [27] Y.Y. Liang, M. Khazaei, A. Ranjbar, M. Arai, S. Yunoki, Y. Kawazoe, H.M. Weng, Z. Fang, Theoretical prediction of two-dimensional functionalized MXene nitrides as topological insulators, *Phys. Rev. B* 96 (2017) 195414.
- [28] S.J. Zhao, W. Kang, J.M. Xue, Manipulation of electronic and magnetic properties of M_2C ($\text{M} = \text{Hf}, \text{Nb}, \text{Sc}, \text{Ta}, \text{Ti}, \text{V}, \text{Zr}$) monolayer by applying mechanical strains, *Appl. Phys. Lett.* 104 (2014) 133106.
- [29] C. Si, J. Zhou, Z. Sun, Half-metallic ferromagnetism and surface functionalization-induced metal-insulator transition in graphene-like two-dimensional Cr_2C crystals, *ACS Appl. Mater. Interfaces* 7 (2015) 17510–17515.
- [30] G. Gao, G. Ding, J. Li, K. Yao, M. Wu, M. Qian, Monolayer MXenes: promising half-metals and spin gapless semiconductors, *Nanoscale* 8 (2016) 8986–8994.
- [31] H. Kumar, N.C. Frey, L. Dong, B. Anasori, Y. Gogotsi, V.B. Shenoy, Tunable magnetism and transport properties in nitride MXenes, *ACS Nano* 11 (2017) 7648–7655.
- [32] A. Chandrasekaran, A. Mishra, A.K. Singh, Ferroelectricity, antiferroelectricity, and ultrathin 2D electron/hole gas in multifunctional monolayer MXene, *Nano Lett.* 17 (2017) 3290–3296.
- [33] M. Khazaei, V. Wang, C. Sevik, A. Ranjbar, M. Arai, S. Yunoki, Electronic structures of iMAX phases and their two-dimensional derivatives: a family of piezoelectric materials, *Phys Rev Mater* 2 (2018) 074002.
- [34] Z.L. Wang, J. Song, Piezoelectric nanogenerators based on zinc oxide nanowire arrays, *Science* 312 (2006) 242–246.
- [35] Z.L. Wang, Piezopotential gated nanowire devices: piezotronics and piezo-phototronics, *Nano Today* 5 (2010) 540–552.
- [36] J. Zhang, C.Y. Wang, C. Bowen, Piezoelectric effects and electromechanical theories at the nanoscale, *Nanoscale* 6 (2014) 13314–13327.
- [37] Y. Wang, Z. Wang, J. Li, J. Tan, B. Wang, Y. Liu, Tight-binding piezoelectric theory and electromechanical coupling correlations for transition metal dichalcogenide monolayers, *Phys. Rev. B* 98 (2018) 125402.
- [38] T. Wu, H. Zhang, Piezoelectricity in two-dimensional materials, *Angew Chem. Int. Ed. Engl.* 54 (2015) 4432–4434.
- [39] J. Zhang, S.A. Meguid, Piezoelectricity of 2D nanomaterials: characterization, properties, and applications, *Semicond. Sci. Technol.* 32 (2017) 043006.
- [40] P. Lin, C. Pan, Z.L. Wang, Two-dimensional nanomaterials for novel piezotronics and piezophototronics, *Materials Today Nano* 4 (2018) 17–31.
- [41] R. Hinchet, U. Khan, C. Falconi, S.W. Kim, Piezoelectric properties in two-dimensional materials: simulations and experiments, *Mater. Today* 21 (2018) 611–630.
- [42] M.N. Blonsky, H.L. Zhuang, A.K. Singh, R.G. Hennig, Ab initio prediction of piezoelectricity in two-dimensional materials, *ACS Nano* 9 (2015) 9885–9891.
- [43] L. Dong, J. Lou, V.B. Shenoy, Large in-plane and vertical piezoelectricity in Janus transition metal dichalcogenides, *ACS Nano* 11 (2017) 8242–8248.
- [44] M.M. Alyoruk, Y. Aierken, D. Cakir, F.M. Peeters, C. Sevik, Promising piezoelectric performance of single layer transition-metal dichalcogenides and dioxides, *J. Phys.*

- Chem. C 119 (2015) 23231–23237.
- [45] K.A.N. Duerloo, M.T. Ong, E.J. Reed, Intrinsic piezoelectricity in two-dimensional materials, *J. Phys. Chem. Lett.* 3 (2012) 2871–2876.
- [46] S.K. Kim, R. Bhatia, T.H. Kim, D. Seol, J.H. Kim, H. Kim, W. Seung, Y. Kim, Y.H. Lee, S.W. Kim, Directional dependent piezoelectric effect in CVD grown monolayer MoS₂ for flexible piezoelectric nanogenerators, *Nano Energy* 22 (2016) 483–489.
- [47] C.J. Brennan, R. Ghosh, K. Koul, S.K. Banerjee, N. Lu, E.T. Yu, Out-of-Plane electromechanical response of monolayer molybdenum disulfide measured by piezoresponse force microscopy, *Nano Lett.* 17 (2017) 5464–5471.
- [48] J. Qi, Y.W. Lan, A.Z. Stieg, J.H. Chen, Y.L. Zhong, L.J. Li, C.D. Chen, Y. Zhang, K.L. Wang, Piezoelectric effect in chemical vapour deposition-grown atomic-monolayer triangular molybdenum disulfide piezotronics, *Nat. Commun.* 6 (2015) 7430.
- [49] H.Y. Zhu, Y. Wang, J. Xiao, M. Liu, S.M. Xiong, Z.J. Wong, Z.L. Ye, Y. Ye, X.B. Yin, X. Zhang, Observation of piezoelectricity in free-standing monolayer MoS₂, *Nat. Nanotechnol.* 10 (2015) 151–155.
- [50] W. Wu, L. Wang, Y. Li, F. Zhang, L. Lin, S. Niu, D. Chenet, X. Zhang, Y. Hao, T.F. Heinz, J. Hone, Z.L. Wang, Piezoelectricity of single-atomic-layer MoS₂ for energy conversion and piezotronics, *Nature* 514 (2014) 470–474.
- [51] K.H. Michel, D. Cakir, C. Sevik, F.M. Peeters, Piezoelectricity in two-dimensional materials: comparative study between lattice dynamics and ab initio calculations, *Phys. Rev. B* 95 (2017) 125415.
- [52] W.B. Li, J. Li, Piezoelectricity in two-dimensional group-III monochalcogenides, *Nano Res* 8 (2015) 3796–3802.
- [53] Y. Guo, S. Zhou, Y.Z. Bai, J.J. Zhao, Enhanced piezoelectric effect in Janus group-III chalcogenide monolayers, *Appl. Phys. Lett.* 110 (2017) 163102.
- [54] R.X. Fei, W.B. Li, J. Li, L. Yang, Giant piezoelectricity of monolayer group IV monochalcogenides: SnSe, SnS, GeSe, and GeS, *Appl. Phys. Lett.* 107 (2015) 173104.
- [55] L.C. Gomes, A. Carvalho, A.H.C. Neto, Enhanced piezoelectricity and modified dielectric screening of two-dimensional group-IV monochalcogenides, *Phys. Rev. B* 92 (2015) 214103.
- [56] P.Z. Hanakata, A. Carvalho, D.K. Campbell, H.S. Park, Polarization and valley switching in monolayer group-IV monochalcogenides, *Phys. Rev. B* 94 (2016) 035304.
- [57] H.B. Yin, J.W. Gao, G.P. Zheng, Y.X. Wang, Y.C. Ma, Giant piezoelectric effects in monolayer group-V binary compounds with honeycomb phases: a first-principles prediction, *J. Phys. Chem. C* 121 (2017) 25576–25584.
- [58] L.C.L.Y. Voon, M. Willatzen, Z.L. Wang, Model calculation of the piezoelectric coefficient of hexagonal 2D materials, *Adv Theor Simul* 2 (2019).
- [59] M.T. Ong, E.J. Reed, Engineered piezoelectricity in graphene, *ACS Nano* 6 (2012) 1387–1394.
- [60] L. Wang, S. Liu, Z. Zhang, X. Feng, L. Zhu, H. Guo, W. Ding, L. Chen, Y. Qin, Z.L. Wang, 2D piezotronics in atomically thin zinc oxide sheets: interfacing gating and channel width gating, *Nano Energy* 60 (2019) 724–733.
- [61] P. Scheeper, A. Van der Donk, W. Olthuis, P. Bergveld, A review of silicon microphones, *Sensor Actuat A-Phys* 44 (1994) 1–11.
- [62] Z.L. Wang, Self-powered nanosensors and nanosystems, *Adv. Mater.* 24 (2012) 280–285.
- [63] Z.B. Yang, S.X. Zhou, J. Zu, D. Inman, High-Performance piezoelectric energy harvesters and their applications, *Joule* 2 (2018) 642–697.
- [64] H.C. Liu, J.W. Zhong, C. Lee, S.W. Lee, L.W. Lin, A comprehensive review on piezoelectric energy harvesting technology: materials, mechanisms, and applications, *Appl. Phys. Rev.* 5 (2018) 041306.
- [65] A.A.M. Noor, H.J. Kim, Y.H. Shin, Dipolar polarization and piezoelectricity of a hexagonal boron nitride sheet decorated with hydrogen and fluorine, *Phys. Chem. Chem. Phys.* 16 (2014) 6575–6582.
- [66] L. Hu, X.R. Huang, Peculiar electronic, strong in-plane and out-of-plane second harmonic generation and piezoelectric properties of atom-thick alpha-M₂X₃ (M = Ga, In; X = S, Se): role of spontaneous electric dipole orientations, *RSC Adv.* 7 (2017) 55034–55043.
- [67] F. Zahid, L. Liu, Y. Zhu, J. Wang, H. Guo, A generic tight-binding model for monolayer, bilayer and bulk MoS₂, *AIP Adv.* 3 (2013).
- [68] G.B. Liu, W.Y. Shan, Y.G. Yao, W. Yao, D. Xiao, Three-band tight-binding model for monolayers of group-VIB transition metal dichalcogenides, *Phys. Rev. B* 88 (2013) 085433.
- [69] E. Cappelluti, R. Roldan, J.A. Silva-Guillen, P. Ordejon, F. Guinea, Tight-binding model and direct-gap/indirect-gap transition in single-layer and multilayer MoS₂, *Phys. Rev. B* 88 (2013) 075409.
- [70] M. Born, K. Huang, *Dynamical Theory of Crystal Lattices*, Clarendon press, 1954.
- [71] D. Cakir, F.M. Peeters, C. Sevik, Mechanical and thermal properties of h-MX₂ (M = Cr, Mo, W; X = O, S, Se, Te) monolayers: a comparative study, *Appl. Phys. Lett.* 104 (2014) 203110.
- [72] J.W. Jiang, J.S. Wang, B.W. Li, Young's modulus of graphene: a molecular dynamics study, *Phys. Rev. B* 80 (2009) 113405.
- [73] M. Zelisko, Y. Hanlumuang, S. Yang, Y. Liu, C. Lei, J. Li, P.M. Ajayan, P. Sharma, Anomalous piezoelectricity in two-dimensional graphene nitride nanosheets, *Nat. Commun.* 5 (2014) 4284.
- [74] J. Shi, Y. Gao, X.L. Wang, S.N. Yun, Electronic, elastic and piezoelectric properties of two-dimensional group-IV buckled monolayers, *Chin. Phys. Lett.* 34 (2017) 087701.
- [75] M.M. Alyoruk, Piezoelectric properties of monolayer II-VI group oxides by first-principles calculations, *Phys. Status Solidi B* 253 (2016) 2534–2539.
- [76] M.T. Ong, K.A.N. Duerloo, E.J. Reed, The effect of hydrogen and fluorine coadsorption on the piezoelectric properties of graphene, *J. Phys. Chem. C* 117 (2013) 3615–3620.
- [77] S. Kumar, U. Schwingschlogl, Thermoelectric performance of functionalized Sc₂C MXenes, *Phys. Rev. B* 94 (2016) 035405.
- [78] G. Kresse, J. Furthmüller, Efficient iterative schemes for ab initio total-energy calculations using a plane-wave basis set, *Phys. Rev. B* 54 (1996) 11169.
- [79] J.P. Perdew, A. Zunger, Self-interaction correction to density-functional approximations for many-electron systems, *Phys. Rev. B* 23 (1981) 5048.
- [80] J.P. Perdew, K. Burke, M. Ernzerhof, Generalized gradient approximation made simple, *Phys. Rev. Lett.* 77 (1996) 3865.
- [81] P.E. Blöchl, Projector augmented-wave method, *Phys. Rev. B* 50 (1994) 17953.
- [82] G. Kresse, D. Joubert, From ultrasoft pseudopotentials to the projector augmented-wave method, *Phys. Rev. B* 59 (1999) 1758.
- [83] M. Marsman, J. Paier, A. Stroppa, G. Kresse, Hybrid functionals applied to extended systems, *J. Phys. Condens. Matter* 20 (2008) 064201.
- [84] X. Gonze, First-principles responses of solids to atomic displacements and homogeneous electric fields: implementation of a conjugate-gradient algorithm, *Phys. Rev. B* 55 (1997) 10337.
- [85] S. Baroni, S. de Gironcoli, A. Dal Corso, P. Giannozzi, Phonons and related crystal properties from density-functional perturbation theory, *Rev. Mod. Phys.* 73 (2001) 515.
- [86] M. de Jong, W. Chen, H. Geerlings, M. Asta, K.A. Persson, A database to enable discovery and design of piezoelectric materials, *Sci Data* 2 (2015) 150053.
- [87] S.P. Timoshenko, S. Woinowsky-Krieger, *Theory of Plates and Shells*, McGraw-hill, 1959.
- [88] S.P. Koenig, N.G. Boddetti, M.L. Dunn, J.S. Bunch, Ultrastrong adhesion of graphene membranes, *Nat. Nanotechnol.* 6 (2011) 543–546.
- [89] X.M. Wang, H. Tian, W.G. Xie, Y. Shu, W.T. Mi, M.A. Mohammad, Q.Y. Xie, Y. Yang, J.B. Xu, T.L. Ren, Observation of a giant two-dimensional band-piezoelectric effect on biaxial-strained graphene, *NPG Asia Mater.* 7 (2015).
- [90] C. Lee, X. Wei, J.W. Kysar, J. Hone, Measurement of the elastic properties and intrinsic strength of monolayer graphene, *Science* 321 (2008) 385–388.



Jie Tan is a research staff at Sino-French Institute of Nuclear Engineering and Technology in Sun Yat-sen University (China). She obtained her Ph.D. degree in Condensed Matter Physics from Shandong University (China) in June 2016. Her research interests mainly focus on the electronic properties, transport properties and electromechanics of nanomaterials (e.g., graphene, MOF and MXene) based on first-principle calculations and nonequilibrium green's function. Recently, she has been paying more attention to the engineering applications of these advanced materials in energy harvesting and piezoelectric sensing.



Yunhua Wang earned his Ph.D. degree in condensed matter physics from Sun Yat-sen University, China, in 2014. He is currently a postdoctoral research fellow with Prof. Shengjun Yuan and Prof. Hai-Qing Lin at Beijing Computational Science Research Center and Prof. Mikhail I. Katsnelson at Radboud University, the Netherlands. His current research interests include electronic, piezoelectric, thermoelectric, ferroelectric, magnetic, mechanical and optical theories and calculations in 2D materials and quantum materials.



Zongtan Wang received his B.S. degree in engineering mechanics from Sun Yat-Sen University in 2013. He is currently a PhD candidate under the supervision of Prof. Y.-L. Liu. His research interests focus on the microscopic piezoelectric theory and strain effects on electronic transports in 2D materials and topological materials.



Xiujie He is an associate professor at Sino-French Institute of Nuclear Engineering and Technology, Sun Yat-sen University (China). He obtained his Ph.D. degree in Condensed Matter Physics from Shandong University (China) in June 2014. Then he finished the postdoctoral research in Tsinghua University from 2014 to 2016. His researches mainly focus on the oxidation and mechanical properties of coating materials. His investigations are carried out by using physical vapor deposition method combined with first-principle calculations.



Yulan Liu is a professor at School of Aeronautics and Astronautics, Sun Yat-sen University (China). She obtained her Ph.D. degree in composite material from Harbin Institute of Technology (China) in 2002. Her research interests mainly focus on the functional materials and engineering applications.



Biao Wang is the Cheung Kong Chair Professor and the Dean of Sino-French Institute of Nuclear Engineering and Technology, Sun Yat-sen University, China. He received his Ph.D. from Harbin Institute of Technology, China in 1988, and then was a post-doctoral fellow in Tsinghua University and IFP, France. From 1994 to 2004, he became a full professor in Harbin Institute of Technology. In June 2004, he joined Sun Yat-sen University as the First-Level Talent and then was the Dean of School of Physics and Engineering of Sun Yat-sen University from 2005 to 2014. His research interest is on the theoretical modeling on the mechanical and functional behaviors of advanced materials. He has won various academic awards, including ISI "Citation Classic Award", the National Excellent Young Investigator

Fund of NSFC, etc.



Mikhail I. Katsnelson is a professor at Radboud University, Nijmegen, the Netherlands. He obtained his bachelor and PhD from Ural State University in 1977 and 1980. From 1977 to 2001 he was working in the Institute of Metal Physics in Ekaterinburg in Russia and hold a position as the head of the group of Quantum Theory of Metals. He became the youngest physicist - Doctor of Sciences in the Soviet Union (1985) and received Lenin Komsomol Prize, the State Prize for young researchers (1988). After working for several years as a visiting professor in Uppsala University (Sweden), in 2004, he became professor of theoretical physics and head of the group of Theory of Condensed Matter in Radboud University. His research interests include many fields of physics, from foundations of quantum mechanics to applications of statistical physics in biology. His best-known achievements are in the theory of graphene, magnetism and strongly correlated systems. He is awarded by Spinoza Prize, Hamburg Prize in Theoretical Physics and by Royal decoration as a Knight of the Order of the Netherlands Lion. Prof. Katsnelson is elected member of Royal Netherlands Academy of Arts and Sciences, Academia Europaea and Royal Society of Sciences at Uppsala and honorary doctor of Uppsala University.



Shengjun Yuan is a professor at Wuhan University, China. He received his BSc in Physics from Zhejiang University (China) in 2001, MSc in theoretical physics from University of Siegen (Germany) in 2003 and PhD in computational physics from University of Groningen (The Netherlands) in 2008. His focus is mainly on the development of numerical methods in computational physics. His research interests include the large-scale simulation of complex quantum systems, periodic and non-periodic low-dimensional quantum systems, modeling of quantum spin systems and universal quantum computers.